Embedding eddy current sensors into LPBF components for structural health monitoring

Author(s):
Stoll, Philipp; Gasparin, Enrico; Spierings, Adriaan; Wegener, Konrad

Publication date:
2021-08

Permanent link:
https://doi.org/10.3929/ethz-b-000495644

Originally published in:
Progress in Additive Manufacturing 6(3), https://doi.org/10.1007/s40964-021-00204-3

Progress in Additive Manufacturing (2021) 6:445–453
https://doi.org/10.1007/s40964-021-00204-3

FULL RESEARCH ARTICLE

Embedding eddy current sensors into LPBF components for structural health monitoring

Philipp Stoll[1] · **Enrico Gasparin**[2] · **Adriaan Spierings**[1] · **Konrad Wegener**[3]

Received: 26 May 2020 / Accepted: 19 June 2021 / Published online: 3 July 2021

Abstract
Laser powder bed fusion (LPBF) facilitates the integration of external elements like sensors into workpieces during manufacturing. These embedded components enable e.g. part monitoring, thus being a fundamental application of industry 4.0. This study assesses the feasibility of embedding eddy current (EC) sensors for non-destructive testing (NDT) into SLM components aiming at structural health monitoring (SHM). A reliable embedding process for EC sensors is developed, ensuring the survivability of the sensors for the LPBF process and its harsh conditions. The experiments conducted demonstrate the possibility to use the embedded EC sensor to observe and detect a controlled crack growth. The cracks are realized either with direct EDM cutting or on the course of a fatigue test of CT specimens. The data retrieved by the embedded EC sensors are proven to provide a direct information about the severity of a damage and its evolution over time for both approaches. Thus, supporting the validation of such an innovative and promising SHM concept.

Keywords Laser powder bed fusion (LPBF) · Sensor Integration · Embedding · Eddy current (EC) inspection · Structural health monitoring (SHM) · Non-destructive testing (NDT)

1 Motivation and vision

Structural health monitoring (SHM) is a very promising approach for lifetime assessment and maintenance activities of mechanically loaded parts since it investigates the components' material integrity. Hence, the predictive maintenance approach according to Matyas [1] can be applied. Compared to other maintenance concepts, predictive maintenance is significantly cheaper because in condition based or periodic maintenance the components are replaced too early as shown by Ryll and Freund [2]. In general, the quality of the acquired data is of significant importance for gaining benefits of the predictive maintenance approach. Often, however, conventional manufacturing technologies permit the positioning of sensors merely in locations, which are too far away from the region of interest for data acquisition. Hence, the data are not as meaningful as they have to be to determine optimal maintenance cycles. This drawback regarding sensor positioning can be mitigated by laser powder bed fusion (LPBF) technology. It enables the integration and precise positioning of sensors into metallic components, as presented conceptionally by Lehmhus et al. [3, 4] and shown practically among others by Petrat et al. [5] for electronic components, e.g. an LED, Stoll et al. [6] for temperature sensors and Maier et al. [7], Mathew et al. [8], Stoll et al. [9] for optical fibers. Among the available Non-Destructive Testing (NDT) technologies, the Eddy Current (EC) technique presents some advantages, such as robustness, absence of requirements for surface preparation or use of couplants, which might alter. In addition, also compact solutions adapted for the integration into Structural Health Monitoring (SHM) applications, as shown by Gasparin et al. [10], can be beneficial for the embedding in LPBF parts.

The aforementioned advantages of EC sensor technology lead to the vision schematically visualized in Fig. 1a, where the embedded sensor will continuously monitor the area with respect to developing cracks. The

✉ Philipp Stoll
stoll@inspire.ethz.ch

[1] Inspire, Innovation Center for Additive Manufacturing Switzerland (Icams), Lerchenfeldstrasse 3, 9014 St. Gallen, Switzerland

[2] Sensima Inspection Sarl, 31 Av. Mont Blanc, 1196 Gland, Switzerland

[3] Institute of Machine Tools and Manufacturing (IWF), Swiss Federal Institute of Technology, ETH Zurich, Leonhardstrasse 21, 8092 Zurich, Switzerland

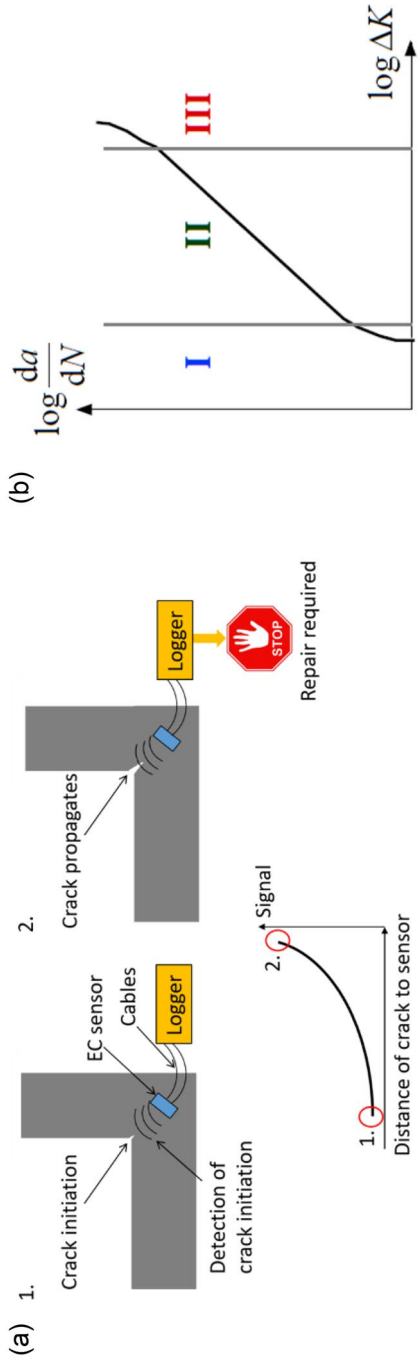

Fig. 1 **a** Vision for structural health monitoring (SHM) of LPBF components by crack detection with EC sensors; b) crack growth as a function of stress intensity factor range ΔK, modified based on [11]

sensor is positioned in a location, where a crack initiation is expected, e.g. based on FEM simulations. Thus, providing real-time data of the crack dimensions. It can be easily thought how the acquired data can be used to trigger alarms and plan repairs or replacements according to the actual health state of the part. Consequently, this approach, which is an exemplary application of industry 4.0, enables an optimal use of the component: the use phase is long enough to prevent changing still faultless components, but it is also short enough to prevent having an expensive machine downtime due to a failure of the component. In Fig. 1b, the fatigue crack growth da/dN, with load cycle number N and crack length a, is plotted as a function of stress intensity factor range ΔK. In sector II, the fatigue cracks grow at a stable rate. This typical behavior of crack propagation is particularly important for the vision presented in Fig. 1a. Despite the non-uniform crack propagation in sectors I and III, it is a valid approach to observe crack propagation with embedded sensors for a certain time and define a maximum crack length as a threshold for initiating the next maintenance cycle, if the major part of the component's fatigue life lies within sector II.

2 Materials and methods

2.1 Eddy current sensor working principle

If a coil inductor is powered with alternating current (AC), an alternating magnetic field is also generated. When the coil approaches a conductive material, EC are generated within the material due to the law of induction. These EC lead to the formation of a magnetic field that is counteracting the primary magnetic field of the coil, therefore affecting its equivalent impedance. The path and intensity of these circulating currents are conditioned by the material properties and the presence of defects such as cracks or porosity; a representation of the EC is schematically visualized in Fig. 2a. As in typical NDT usage, the impedance is expressed with real and imaginary part in normalized units and represented on the complex plane (see Fig. 2b). The characteristic curve depends on the material properties (conductivity σ, permeability μ) as well as on the sensor parameters (coil radius a, angular frequency ω). In Fig. 2b, it is also shown that the detection of a crack leads to a significantly different trajectory than the detection of a liftoff between sensor and material to be tested, which enables to distinguish among the interest signal features. A deeper insight to the functionality of EC sensors technology for NDT is given in [12].

For the experimental study, only the EC sensors are embedded in the LPBF parts, whereas the electronics for data acquisition and signal processing are positioned

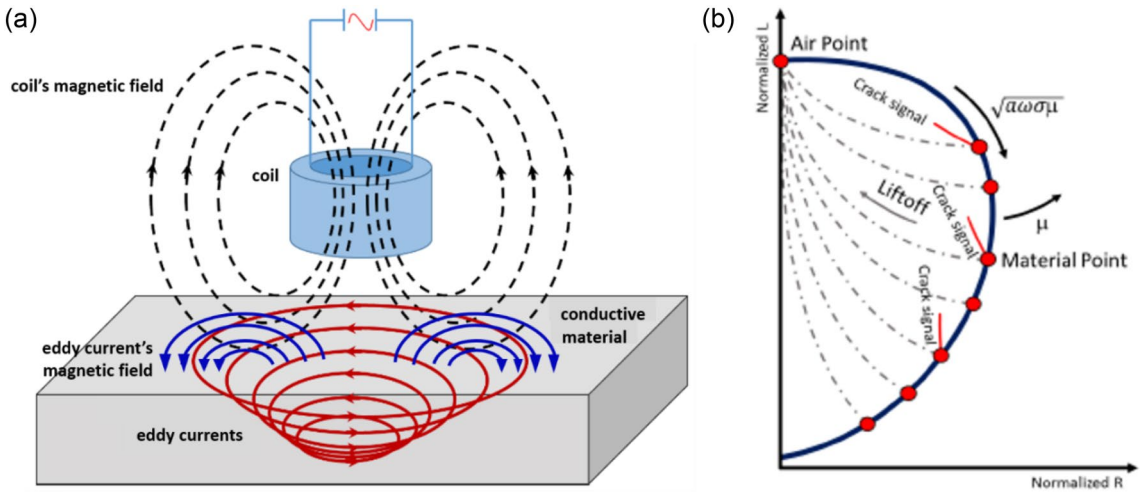

Fig. 2 **a** working principle—generation of EC in conductive material; modified based on Hippert [13]; **b** impedance plane for data representation from Hippert [13]

outside. Nevertheless, the integration of the electronics into the LPBF part could also be possible, as the necessary elements would fit in an extremely small volume, comparable to the size of the sensor itself. All these components were provided by Sensima inspection Sarl [14]. The instrument provides a direct readout of the real and imaginary parts related to the variation of the coil impedance, expressed in arbitrary units (a.u.), as typically used by NDT inspectors.

2.2 Sensor embedding

A Concept Laser m2-machine equipped with a Nd:YAG laser with 1064 nm wavelength and maximum power of 400 W operating in cw-mode was used for the manufacturing of the test specimens. The parts were manufactured from SS 316L powder with a standard process parameter set ($P_{\text{Laser}} = 180$ W, scan speed $v_{\text{scan}} = 1350$ mm/s, hatch distance $h = 75$ µm, layer thickness $t = 30$ µm, with O_2 atmosphere and without base plate heating) leading to relative part densities > 99.0% compared to the reference of 7.95 g/cm^3 given in the certification of the supplier, Carpenter Powder Products. SS 316L is a beneficial material for the measurement of embedded cracks with EC, since the low magnetic permeability ($\mu_{\text{rel}} = 1.25$ [15]) allows a larger penetration depth of the induced currents compared to materials with higher permeability. The embedded sensor configuration offers a sensitivity for crack detection up to 3.5 mm.

In Fig. 3, the cavity design for sensor embedding is schematically visualized**.** Figure 3a shows the CAD model used for the manufacturing of the component, while Fig. 3b and c schematically represent the demonstrator and in particular the direction of crack growth with respect to the position of the sensor. The EC sensor with a diameter of 3.3 mm is placed inside a cylindrical cavity with a diameter of 5.0 mm, i.e. there is a circular clearance of 0.85 mm between sensor and cavity to account for the roughness of the LPBF surfaces. The cavity is closed gently with an overhanging surface (see Fig. 3). Such structure has no influence on the EC measurements since the sensor is directional, i.e. the major region of sensitivity is oriented toward the location of crack initiation during the experiments. To achieve a proper positioning, the EC sensor is pressed to the bottom of the cavity and subsequently held in place by filling the entire cavity with a quick hardening resin (Plus 2-K-Epoxidkleber from UHU). While this process does not require any special attention, the outlet of the copper wires from the LPBF component needs to be designed properly. The wires forming the coils are only 60 µm in diameter, including an epoxy insulation to prevent a short circuit. Due to these small dimensions, for the use phase of the part the wires have to be protected from the sharp edges of the LPBF component. Hence, a heat shrink tube is inserted into the horizontally orientated cable channel preventing any contact between the wires and the LPBF part. In Fig. 4, the sensor integration process is shown. The epoxy insulation of the copper wires also limits the maximum temperature the sensor system can withstand, as at temperatures above 250 °C the insulation would melt, resulting in a short circuit between the wires and the LPBF component. The continuation of the LPBF process does not require any special precautions. It is expected that there is an impact of the interruption of the process on the structural integrity of the component. However, this field of research was not in the scope of this work focusing on the process of sensor embedding and sensor survivability.

After the LPBF process, the fine copper wires are soldered to shielded twisted pair cables suitable for the interaction with the data processing unit. In addition, to prevent a rupture of either the thin copper wires or the soldering

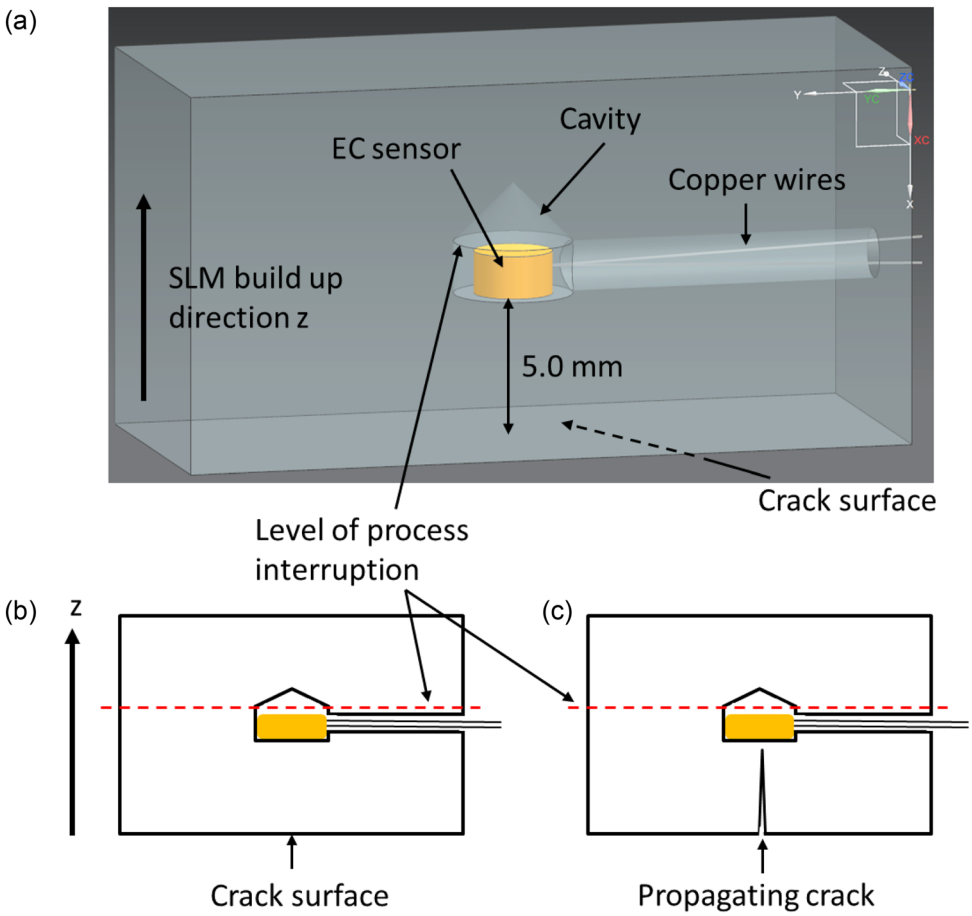

Fig.3 **a** CAD model of the demonstrator with dedicated cavity design for integration of EC sensors; **b** schematic representation of the demonstrator prior to crack initiation; **c** schematic representation of the demonstrator showing the crack propagating towards the embedded sensor

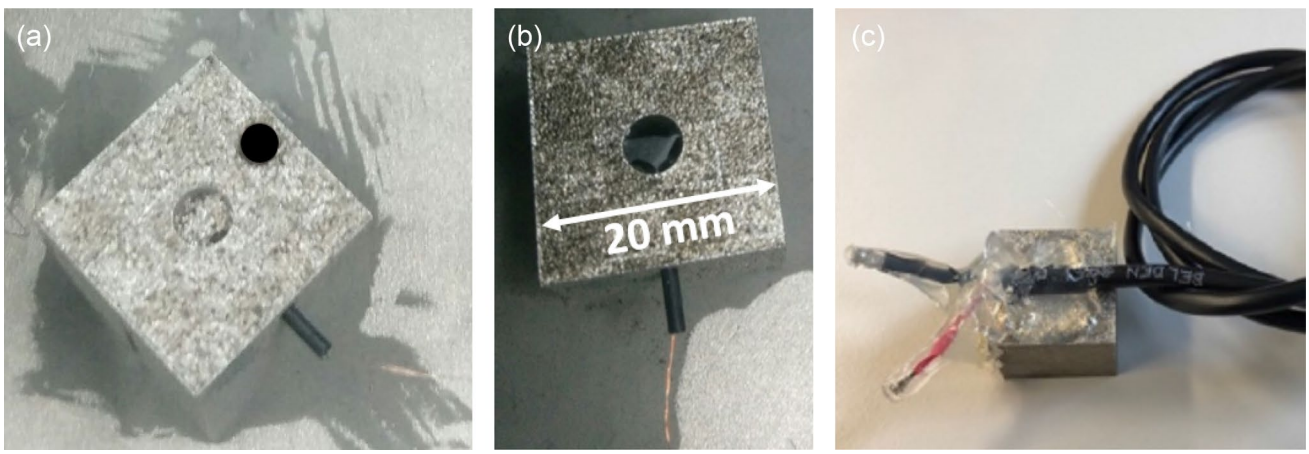

Fig.4 Sensor integration process for EC sensors: **a** powder removal, insertion of heat shrink tubes as wire protection and leading of wires through heat shrink tubes; **b** integration of the EC sensor into the cavity and application of resin to fix the sensor in its position; **c** LPBF test specimens with soldered cables, ready to be tested

region, all is encapsulated and protected by a layer of hot-melt adhesive, thus ensuring a good mechanical fixation also against any vibration. Figure 4c shows an LPBF test part with an embedded EC sensor ready to be tested.

3 Measurement setup

To validate the application of embedded EC sensors in LPBF a controlled crack growth is provoked in the

specimens. Consequently, the EC data acquired during the whole experiments are compared to the length of the propagated crack. The crack is propagated from the specimen's external surface until reaching the EC sensor, in the z sensor axis (with respect to LPBF build-up direction in Fig. 3). Within the framework of this study, the crack initiation and propagation were achieved with two different experimental setups.

3.1 Wire-electrical discharge machining (EDM)

In this setup, the crack that is propagating towards the embedded sensor and is detected by the sensor is generated by a wire EDM cut. The machine for the tests is an Agie Charmilles Technologies type Robofil 4030SI-TW with a wire of 250 µm diameter. Although this dimension deviates significantly from a typical crack width that the embedded EC sensors should detect, it perfectly fulfils the requirements for the experiment. Generally, the width of the crack to be detected is not that important since it is more than an order of magnitude smaller than the diameter of the coil. Although the wire-cut EDM machine provides information on the current position of the wire, the data acquisition has to be done in variable discrete steps from 50 to 100 µm during the pausing of the cutting. Otherwise, the very strong currents of the wire-EDM process significantly disturb the EC sensor signal. The specimens were cut until the wire was reaching the sensor surface, which cannot be cut as it is from insulating material. This condition, verified visually by the operator, was used to determine the effective crack length. Unfortunately, this procedure suffers from uncertainty, estimated to ± 0.25 mm, due to the difficulties in ensuring the parallelism of the specimen surface with respect to the cutting axis.

3.2 Compact tension (CT) specimens

In the second experiment, EC sensors were embedded in CT specimens usually used for crack propagation analysis in material characterization. Hence, this setup is distinctly closer to real crack growth behavior. The general design and dimensions of a CT specimen according to ASTM E1681 [16] are depicted in Fig. 5a. *Z* indicates the LPBF build-up direction and the sensor within the cavity is also shown. With LPBF, merely blocks were manufactured, while the final geometry was realized by wire-EDM. In the test cycle, the CT specimens were cyclically loaded to initiate and propagate a crack. The machine used for the tests is a Rumul Testronic 100 kN from Russenberger Prüfmaschinen AG. During the measurements, it operated at a maximum frequency of 55.6 Hz and a maximum load of 6.11 kN. In Fig. 5b, the propagating crack is clearly visible. As for the wire-EDM process, the data points were measured discretely, regularly stopping the machine. The step size was defined by a frequency drop of 1.0 Hz, which is a machine-specific value and which was upfront correlated to a crack propagation of ≈1 mm. The evaluation of the effective crack length at the discrete stops was done visually by beach mark analysis after the testing, which was controlled by the application of a constant ΔK.

In both experiments (Sects. 2.3.1,2.3.2, EC data are acquired. As previously introduced, the instrument provides a normalized readout of the real and imaginary parts of the coil impedance. In Fig. 7**,** the raw data collected during an experiment are visualized on the complex plane, showing the characteristic variation of the impedance signal of an EC sensor with respect to the crack growth. The modulus of the impedance variation since the beginning of the experiment until the full crack growth is the quantity used for all the subsequent evaluations. This quantity also referred to as the "EC signal" in the graphs, represents the sensor response to the embedded crack growth. An example of this curve can be observed in Fig. 6. It should be noted that the sensitivity is a function of the distance to the sensor and it increases when the defect gets closer to the sensor, according to the distribution of the induced currents. It follows, that the inverse function of this curve can be used for a direct estimation of the crack to sensor distance, provided in input the EC signal, as could be more desirable for a final application. Some further data processing can be applied without a doubt to this purpose, but this is not in the scope of the paper at hand and is left to future works.

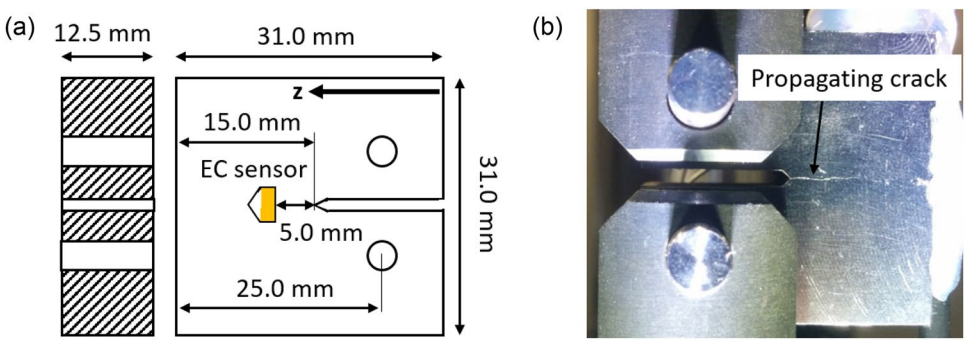

Fig. 5 **a** General dimensions of CT specimen according to ASTM E 1681 [15]; **b** propagating crack during cyclic loading

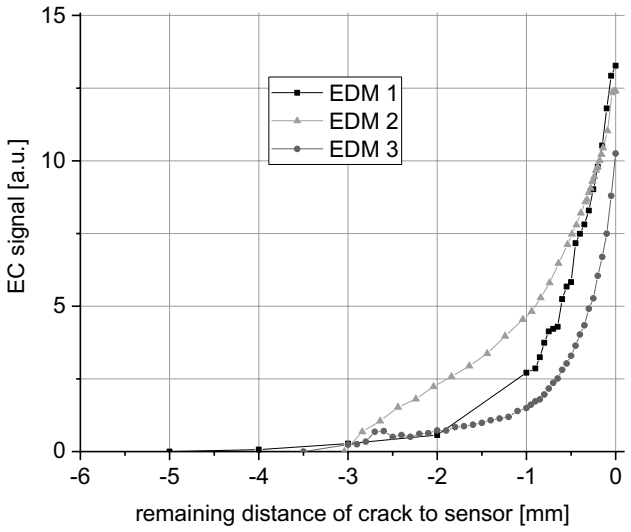

Fig. 6 Results of the EDM wire cut experiments with a controlled crack growth over a set of three specimens. The graph reports the EC signal variation with respect to the distance among crack and sensor. The sensitivity to cracking can be identified at approximatively 2.8 ± 0.3 mm from the sensor surface. The signal variation with respect to the crack growth increases while approaching the sensor

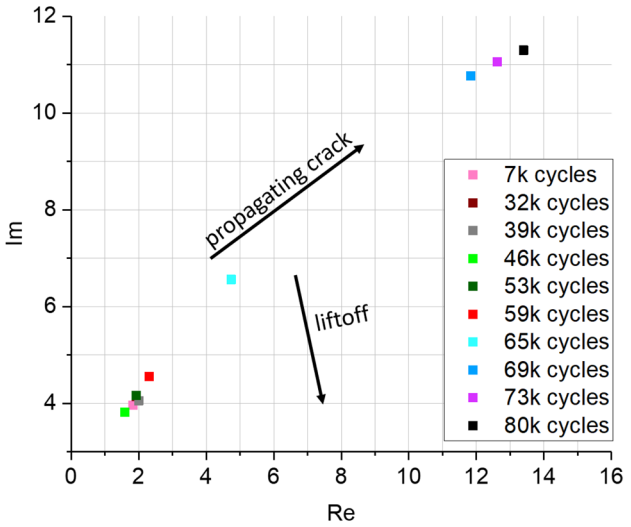

Fig. 7 Raw EC sensor data sampling points represented on the impedance plane resulting from the fatigue testing on a CT specimen for different cumulative load cycles. In addition, the trends of the data points due to the crack propagation and liftoff are indicated

4 Results and discussion: measurement of crack propagation

In a first step, the EC sensors' survivability of the embedding process is evaluated. Due to the orientation of the EC sensor and the embedding concept, these are not damaged by the laser beam or the heat induced into the parts during LPBF process continuation. Instead, the handling of the thin copper wires during soldering of thicker cables and during machining of the test specimens imposes the biggest risk regarding sensor destruction. The integrity of the embedded sensors was verified measuring the coil impedance before and after embedding. Several prototypes were manufactured and a negligible variance of less than 1.5% of nominal impedance was observed. This effect is also partly due to the variation of the magnetic environment of the sensor surrounded by SS 316L. Such deviation is considered negligible and not affecting the purposes of the experiments. A campaign of experiments over several specimens was conducted, in all cases showing comparable trends.

In Fig. 6, the crack propagation results are presented for the three specimens, for which the cracks were generated by wire-EDM process. The horizontal axis shows the remaining distance between the crack and the embedded EC sensor, i.e. at 0.0 mm the crack has reached the sensor. In the graph, the curves correspond to the modulus of the relative impedance variation with respect to the reference point at the start of the experiment. Focusing for instance on the sample "EDM1", the line exhibits an almost linear trend up to a distance of 1.0 mm between crack and sensor, increasing dramatically afterwards. The data shows that the embedded EC sensor can detect a crack approaching it, as assumed in the SHM vision (see Fig. 1a). For the other two samples, similar trends are observed, in spite of the dispersion of the EC signals. Such variations can be explained with a misalignement, the positioning tolerance of the sensor within the cavity (leading to a shift on the x-axis of the graph), or simply due to the different relative positions of the defect with respect to the sensing zone. Nevertheless, such effects do not compromise the possibility to detect the crack initiation and its grow rate in the volume covered by the sensor. An empirical and sufficiently conservative threshold of 0.5% of the instrument full-scale range, (i.e. 100 a.u.), is considered for the raw unfiltered data to determine the largest distance from the sensor at which cracking is detected. Considering the mean value calculated over the set of EDM specimens tested, this threshold is reached at a distance of 2.8 ± 0.3 mm between crack and sensor, where 0.3 mm is the maximum deviation.

For what concern the fatigue tests of CT specimens, the EC signal measured as a function of the applied cumulative load cycles, hence, of the crack length can be observed in Fig. 7 for a representative specimen. The plot clearly reveals a drift for the discrete data points in the typical direction of a propagating crack. The cluster of data points in the lower-left corner, corresponding to measurements with up to 53 k load cycles, are confined in a confidence boundary of 0.5% of the full-scale range, meaning that yet no crack propagation has been detected. From 59 k cycles onwards, the effect

of crack propagation can be easily noticed; the data samples migrate towards a preferential direction, until reaching the maximum distance from the starting point at 80 k cycle (top right corner of the graph), when the experiment was stopped. The data presented in Fig. 7 was further processed to calculate the relative impedance variation and compared to other measured quantities. In Fig. 8, the number of cycles (b) and the EC signal (c) are plotted over the estimated crack length for two tested specimens. In c), it is possible to observe a variation of more than 0.5% at about 2.8 mm from the sensor. It is worth to notice that the crack length is a visually determined value from beach mark analysis in this case. During each stop of the cyclic loading of the CT specimens, a beach mark is formed on the fracture surface, which is visible in a post-process analysis. It reveals an uncertainty of ± 0.25 mm. However, a correlation among the EC data and the force applied by the testing machine is observed as the equivalent specimen load carrying cross section reduces (see Fig. 8a), therefore supporting the validation of the sensor capability in monitoring a growing crack.

In both experimental setups, similar results were observed while comparing the obtained curves of EC signals with respect to the estimated distance to the crack. The data sampling during the EDM experiment is based on significantly more points since the wire-EDM process can be done in finer discrete steps from 50 to 100 µm. For the CT specimens, the uncertainty of the distance among sensor and crack is larger, which is particularly attributed to the beach mark analysis for crack length detection. Additionally, the number of samples is coarser due to practical reasons in the operation of the fatigue machine. A view to the whole dataset built from the campaign of experiments over two specimens led all to comparable results in the trend, while comparisons aimed to define the distance, at which the sensor detects the crack, are made harder due to the uncertainty of the crack length estimation. With CT specimens, it should further be noted that the cracks do not always propagate in a straight line. In both experimental setups, it was possible to detect the crack while entering the region of sensitivity of the EC sensor and reconstruct the overall propagation trend until the end of the experiment. At this purpose, the measured EC signal has been compared to the distance between crack and sensor. The amplitude and the slope over time of such quantity provide a direct information on the evolution of the crack propagation in the component.

The deviations observed among the specimens are mainly attributed to the difficulties in performing an accurate measurement of the crack length, which would also enable the sensor calibration and, with further processing, a direct calculation of the crack to sensor distance based on the EC measurement only. Other factors contributing to the uncertainty of the results are the difficulties to guarantee a controlled alignment and distance of the

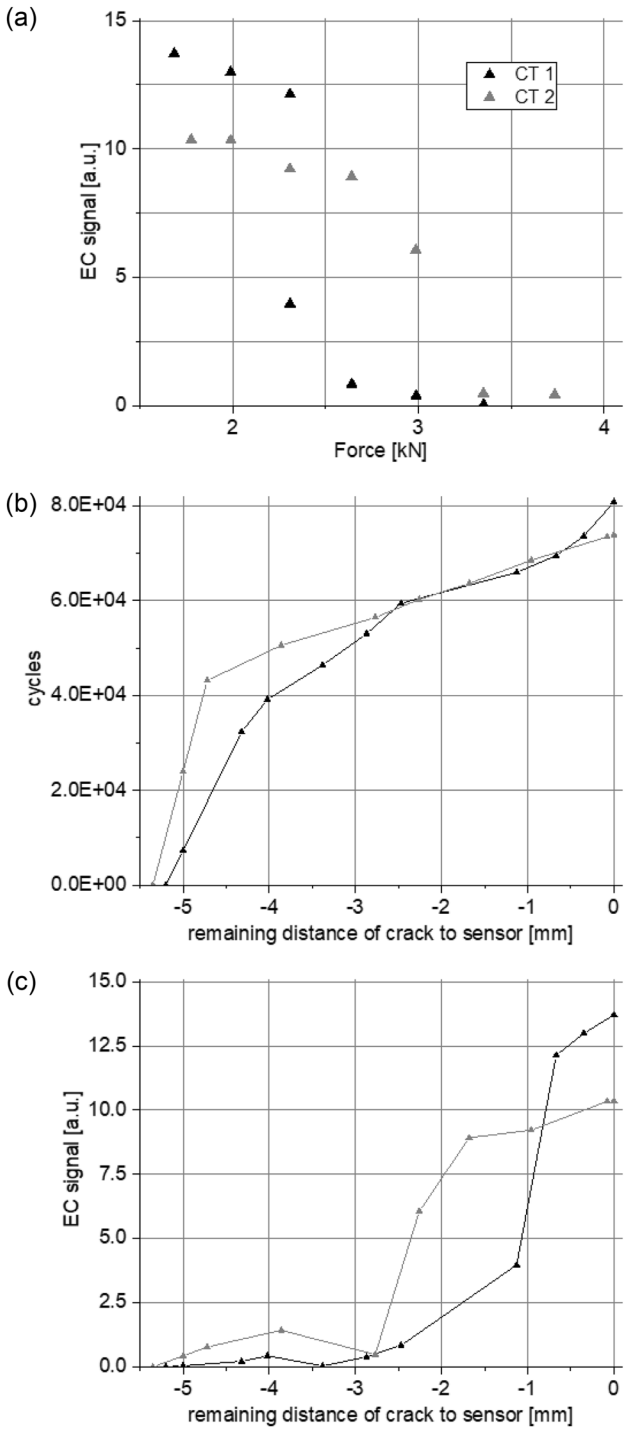

Fig. 8 Results of crack detection with crack initiation and propagation by dynamic testing conducted over two CT specimens; **a** correlation of EC data and the force applied by the testing machine as the equivalent load carrying cross section of the specimen reduces; **b** correlation between load cycles and crack length, expressed as remaining distance of the crack to the embedded sensor; **c** EC signal as a function of the estimated distance between crack tip and sensor

sensor to the surface during the embedding and, to a minor degree, potential variations of the specimen porosity (see Sect. 2.2).

5 Conclusions on embedding of EC sensors

The results presented and discussed in this study highlight the possibility of using embedded EC sensors for SHM of LPBF components. A reliable embedding process for EC sensors was developed. The survivability of the sensors during the LPBF process was critical regarding the fine copper wires, which are insulated with an epoxy layer. Thus, the temperature of the LPBF specimen must not exceed 250 °C during the LPBF process. The timely limited high energy input is obviously not causing any damage to this epoxy insulation. Regarding the outlet of the fine wires (60 µm) from the LPBF components, the protection by heat shrink tubes turned out to be a feasible solution. A campaign of experiments demonstrated the possibility to use the embedded EC sensor to observe and detect a controlled crack growth. The defects were realized either with direct EDM cutting or on the course of a fatigue test of CT specimens. For the CT specimens, the trend can also be compared to the actuation force, showing a correlation between the force drop and the crack growth indication provided by the EC sensor, further supporting the measurements' consistency. The data retrieved by the EC sensors embedded into LPBF parts are proven to provide direct information about the crack propagation and its evolution over time. Nevertheless, further studies could be devoted to enable more advanced estimation of the end-of-lifetime of the components, for instance, using models based on the direct estimation of the crack size.

Acknowledgements The authors like to thank Innosuisse—Swiss Innovation Agency for co-financing the investigations within the frame of an innovation cheque. The authors like to thank Mark Voegtlin (inspire AG) for the excellent work he conducted in the frame of this study and for his imperturbable enthusiasm for further investigations. Special thanks go to Stuart Holdsworth (inspire AG icmi) who supported the authors in a very patient way with his deep expertise in material integrity characterization.

Author contributions Not applicable.

Funding Open Access funding provided by ETH Zurich. The authors like to thank Innosuisse—Swiss Innovation Agency for co-financing the investigations within the frame of an innovation cheque.

Availability of data and material Not applicable.

Code availability Not applicable.

Declarations

Conflict of interest The authors declare that they have no conflict of interest.

References

1. Matyas K (2002) Ganzheitliche optimierung duch individuelle instandhaltungsstrategien. Ind Manag 18(4):13–16
2. Ryll F, Freund C (2010) Grundlagen der instandhaltung. In: Schenk M (ed) Instandhaltung technischer systeme - methoden und werkzeuge zur gewährleistung eines sicheren und wirtschaftlichen anlagenbetriebs. Springer, Berlin, p 23–101. https://doi.org/10.1007/978-3-642-03949-5
3. Lehmhus D, Aumund-Kopp C, Petzoldt F, Godlinski D, Haberkorn A, Zöllmer V, Busse M (2016) Customized smartness: a survey on links between additive manufacturing and sensor integration. Proc Technol 26:284–301. https://doi.org/10.1016/j.protcy.2016.08.038
4. Lehmhus DB, Matthias (2017) Sensor and electronics integration in additive manufacturing. In: Material-integrated intelligent systems—technology and applications. https://doi.org/10.1002/9783527679249.ch9
5. Petrat T, Kersting R, Graf B, Rethmeier M (2018) Embedding electronics into additive manufactured components using laser metal deposition and selective laser melting. Proc CIRP 74:168–171. https://doi.org/10.1016/j.procir.2018.08.071
6. Stoll P, Leutenecker-Twelsiek B, Spierings A, Klahn C, Wegener K (2018) Temperature monitoring of an SLM part with embedded sensor. In: Industrializing additive manufacturing—proceedings of additive manufacturing in products and applications (AMPA2017). Springer, Berlin, p 273–284
7. Maier RRJ, Havermann D, MacPhseronWN, Hand DP (2013) Embedding metallic jacketed fused silica fibres into stainless steel using additive layer manufacturing technology. In: Jaroszewicz LR (ed) Fifth European workshop on optical fibre sensors. SPIE proceedings, p 4. https://doi.org/10.1117/12.2026076
8. Mathew J, Hauser C, Stoll P, Kenel C, Polyzos D, Havermann D, Macpherson W, Hand D, Leinenbach C, Spierings A, Koenig-Urban K, Maier R (2017) Integrating fiber Fabry-Perot cavity sensor Into 3-D printed metal components for extreme high-temperature monitoring applications. IEEE Sens J. https://doi.org/10.1109/JSEN.2017.2703085
9. Stoll P, Mathew J, Spierings A, Bauer T, Maier RRJ., Wegener K (2016) Embedding fibre optical sensors into SLM parts. In: 27th annual international solid freeform fabrication symposium—an additive manufacturing conference, Austin, Texas
10. Gasparin E, Santi G, Nussbaumer A (2015) Eddy current crack monitoring system for structural health monitoring (SHM)

applications. In: 68th international institute for welding (IIW) annual assembly and international conference, Helsinki, Finland
11. Anderson TL (2005) Fracture mechanics: fundamentals and applications, 3rd edn. CRC Press, Taylor & Francis Group, Boca Raton
12. García-Martín J, Gómez-Gil J, Vázquez-Sánchez E (2011) Non-destructive techniques based on eddy current testing. Sensors 11(3):2525–2565
13. Hippert D (2015) High resolution eddy current inspection and eddy current testing for additive manufacturing. Ecole Polytechnique Federale de Lausanne, Lausanne
14. Sensima-Inspection (2019) Private and confidential communication
15. Dubois P-E, Mantel M, Fofanov D, van Bennekom A, Wilke F (2008) Magnetic properties of stainless steels: applications, opportunities and new developments. In: Second international conference on steels in cars and trucks SCT 2008, Wiesbaden, Germany. Stahleisen GmbH, Dusseldorf, pp 314–320
16. ASTM (2013) ASTM E1681-03 (2013) Standard test method for determining threshold stress intensity factor for environment-assisted cracking of metallic materials